Stacked Denoising Autoencoders and Transfer Learning for Immunogold Particles Detection and Recognition

Ricardo Gamelas Sousa[1], Jorge M. Santos[2], Luís M. Silva[3],
Luís A. Alexandre[4], Tiago Esteves[5], Sara Rocha[6], Paulo Monjardino[7],
Joaquim Marques de Sá[8], Francisco Figueiredo[9], and Pedro Quelhas[10]

[1]*Farfetch, Porto, Portugal*
[2]*Instituto Superior de Engenharia, Politécnico do Porto, Portugal*
[3]*Dep. de Matemática at Universidade de Aveiro, Portugal*
[4]*Instituto de Telecomunicações, Universidade da Beira Interior, Rua Marquês d'Ávila e Bolama, 6201-001, Covilhã, Portugal*
[5]*Instituto de Investigaçáo e Inovaçáo em Saúde (i3S) Porto, Portugal*
[6]*Centro de Biotecnologia dos Açores (CBA), Universidade dos Açores, Portugal*
[7]*Centro de Biotecnologia dos Açores (CBA), Universidade dos Açores, Portugal*
[8]*Instituto de Engenharia Biomédica (INEB), Porto, Portugal*
[9]*Instituto de Investigaçáo e Inovaçáo em Saúde (i3S) Porto, Portugal*
[10]*Instituto de Investigaçáo e Inovaçáo em Saúde (i3S) Porto, Portugal*

December 11, 2017

Abstract

In this paper we present a system for the detection of immunogold particles and a Transfer Learning (TL) framework for the recognition of these immunogold particles. Immunogold particles are part of a high-magnification method for the selective localization of biological molecules at the subcellular level only visible through Electron Microscopy (EM). The number of immunogold particles in the cell walls allows the assessment of the differences in their compositions providing a tool to analyse the quality of different plants. For its quantization one requires a laborious manual labeling (or annotation) of images containing hundreds of particles. The system that is proposed in this paper can leverage significantly the burden of this manual task.

For particle detection we use a Laplacian of Gaussian (LoG) filter coupled with a Stacked Denoising Autoencoder (SDA). In order to improve the recognition, we also study the applicability of TL settings

1

for immunogold recognition. TL reuses the learning model of a source problem on other datasets (target problems) containing particles of different sizes. The proposed system was developed to solve a particular problem on maize cells, namely to determine the composition of cell wall ingrowths in endosperm transfer cells. This novel dataset as well as the code for reproducing our experiments is made publicly available.

We determined that the LoG detector alone attained more than 84% of accuracy with the F-measure. Developing immunogold recognition with TL also provided superior performance when compared with the baseline models augmenting the accuracy rates by 10%.

1   Introduction

Immunogold electron microscopy is a high-magnification method for the selective localization of biological molecules at the subcellular level. Antibodies coupled to particles of colloidal gold, which are visible in the transmission electron microscope, can reveal the localization and distribution of biological molecules of interest. In this particular work, this technique was used to determine the composition of cell wall ingrowths of maize (*Zea mays* L.) endosperm transfer cells [27]. Wall ingrowths are uneven thickenings of the cell wall that increase significantly the area of the plasmalemma, thus enabling to sustain a high number of membrane transporters and produce better plants. In addition, INCW2, a cell wall-bound invertase and an essential enzyme for passive sugar flow into the endosperm, is mostly located in the wall ingrowths [19]. Therefore, wall ingrowths contribute significantly to enhance transport capacity of assimilates into the endosperm, thus having a significant impact on kernel yield.

Most basal maize endosperm transfer cells differentiate reticulate ingrowths in the outer periclinal wall and flange ingrowths in the inner periclinal walls and anticlinal walls [27]. This unique feature has not been reported in any other species and makes these cells a unique model to study the differences and similarities of both types of ingrowths and underlying primary cell wall.

In the process of analyzing the cell's ultra-structure it is important to have different magnifications. A wider field of view is achieved with lower magnifications and a more detailed analysis of the cell's ultra-structure is achieved with higher magnifications. In less magnified samples it is more difficult to detect the immunogold particles that are easily confused with cell's ultra-structure, but enable the identification of the larger structures of the cells, namely the ingrowths and adjacent walls (see Figure 1). Higher magnification images provide a detailed analysis of the ultra-structure essential to this study (see also Figure 1 in [34]).

The use of specific antibodies reveals the differences and similarities of components of the walls and ingrowths throughout the development of trans-
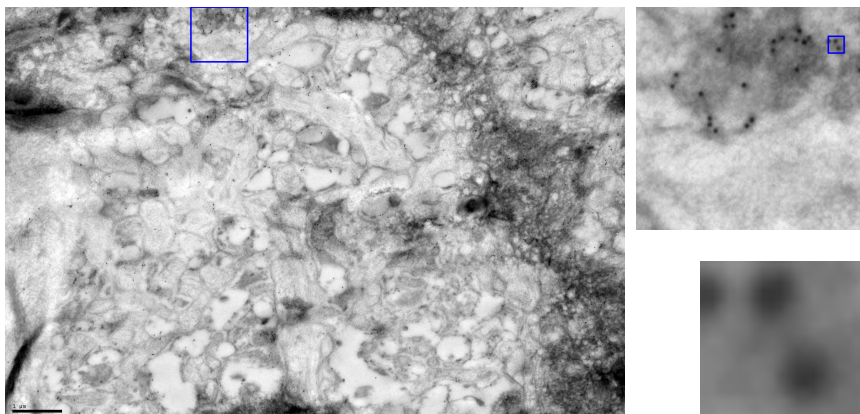
Figure 1: Representative images of our datasets illustrating different structures that can interfere in the recognition of the immunogold particles due to: cellular overlapping, tissues and background noise. Each image has 4008×2670 pixels of dimension with particles' *diameter* ranging from 8 to 20 pixels. In this particular image we have a sample with a magnification of 15000 (scale of $1\mu m$ to the side of the image) with particles with a diameter of 8 pixels. Right to the main figure, we have a magnification of a cluster of immunogold particles with noise and background; in the bottom a magnification of the cluster is also depicted in a 20×20 patch containing two particles.

fer cells. The automatic detection of immunogold particles is a valued tool to facilitate the calculation of the amount of immunogold particles in the walls and ingrowths studied and by that to determine the differences in their composition. One drawback is that the quantification of immunogold particles is a very time-consuming and prone to error task [32] which can benefit from an automatic detection and recognition tool.

Given an approximate size of the immunogold particles radius, we show that the Laplacian of Gaussian (LoG) filter is tolerant to shape variations and to noise that may occur during the image acquisition. The feasibility of this approach is however limited by the quality of the image — see Figure 1. To overcome this constraint, we propose a framework that couples a Stacked Denoising Autoencoder (SDA) to filter the detections of the LoG filter and thus accelerate the whole process. This framework is tolerant to false detections by the LoG filter and afterwards uses the capability of the SDA to extract high representative features from our images towards the improvement of the detection rates [13].

Another proposal of this manuscript refers to how to handle datasets corresponding to immunogold particles captured with different magnifications: one simple way is to devise independent Machine Learning (ML) techniques

so we can analyze each one properly. Transfer Learning (TL) accelerates this process by *reusing* a classifier designed for a given (*source*) problem on another (*target*) problem, with some similarities with the original one [34]. The rationale to apply TL to immunogold particles detection is related to the difficulty to identify these structures, especially in lower magnifications, due to noise, complex structures and annotations with feeble quality. On the other hand, with higher magnifications the distinction between artifacts and structures can be conducted in a easier way due to clear boundaries. For this reason, it is straightforward to explore the advantages of using TL by transferring a model that was obtained on a higher magnification to a dataset of a lower magnification.

The detection and recognition of Cellular Structures and Ultrastructure (CSU) in Electron Microscopy (EM) is still in its infancy. We will still outline some of the few works that have been presented in the literature in Section 2. Our proposal for the detection of immunogold particles using our combined approach with the LoG and SDA will be described in Section 3. Since it is common to acquire samples in different magnifications we explore our hypothesis on the benefits of using TL for immunogold recognition in Section 4. Experimental study and discussion of the results are presented in Section 5 and finally, conclusions are drawn in Section 6.

2   Previous Works

Automatic cellular structure and ultra-structure detection in microscopy imaging has been evolving fast in the literature, mostly due to requirements of processing massive data storages or the emergence of new microscopy technologies [20]. For example, Fisker *et al.* in [12] explore the possibility of automatically estimating particle sizes in immuno-microscopy imaging. Their approach is based on deformable models that can be fitted to the prior known shape of the particles. A different approach was presented by Mallic *et al.* in [25] with the same goal as Fisker, where a cascade of classifiers was employed.

Beyond these works, Ribeiro *et al.* in [32] contributed with an insight review on the processing of images generated by electron microscopies and the advantages of methodologies. Obviously, experimental speed-ups and reproducibility are some of the most mentioned valuable aspects of these tools. In the limit, and since complex structures viewed in EM acquisitions entail a manual analysis of such images by one (or several) experts (which can take several hours or even years to conclude — see page 7 in [20]), this strengthens the motivation for (semi-) automated tools for EM image analysis.

On cryo-electron microscopy images (a technology similar to EM), Voss, Woolford and co-workers [38, 40] applied a Difference of Gaussian (DoG)

4

and LoG filters as a first step to detect biological structures. However, they were not tailored for immunogold particles. For the detection of biological structures, there is an algorithm entitled Spot Detector (SD) [28] that is included in the well-known Icy bioimaging software (Icy, in short) [7]. SD is based on the non-decimated wavelet transform allowing the detection of spots that can be organelles or other biological structures [28]. This approach aggregates a response for each magnification and scale of the image providing detailed information of the objects. A major drawback is concerned with the number of parameters required to function properly (e.g., the identification of a trade-off between particles and background; the definition of a scale and sensibility that controls both size of the particles to be detected and a threshold for noise removal), which may be infeasible for a non-expert user. In a work more closely related to ours, Wang *et al.* [39] explored a DoG approach, a computational cost optimization of LoG, for the detection of immunogold particles on EM images.

Note that automatic organelle detection and identification (segmentation and classification), especially in EM imaging, is relatively recent (see for instance refs. Straehle et al., 2011; Kreshuk et al., 2011 in [20]). For this reason, there are very few works that tackle explicitly the biomedical analysis on EM images. For the segmentation of mitochondria an extension of the super-pixel approach was proposed in Fua *et al.* (see [23] and ref. 17 in [15]) or, as Ciresan *et al.* proposed using Deep Neural Networks (DNNs) [8, 9]. More recently, Huang and co-workers have tackled the detection of other cellular structures based on a symmetry transform [14].

In this paper we will address the detection and recognition of immunogold particles. A major difference from the aforementioned proposals is that organelles are irregular (e.g., in shapes and intensities) and with distinct aspects between themselves. This work is focused on an intuitive tool for the detection of immunogold particles with regular spherical shape, thus avoiding the adoption of a highly parameterized formalism. Moreover, this proposal combines a conventional LoG filter with a Machine Learning algorithm (Transfer Learning with SDAs) improving the results produced by the LoG alone. With the nonexistent (to the best of our knowledge) of an equivalent approach, this work aims to provide a first approach to tackle complex biological structures existing in EM imaging, thus paving the way to other robust machine learning methodologies.

3   Immunogold Particles Detection

We present a cooperative approach for particle detection and recognition. Our approach encompasses coupling the detection performed by a LoG filter and a post-processing stage conducted by a deep learning approach (SDA).

3.1 Immunogold Particle Detection using a LoG Filter

For the task of immunogold particle detection we used the LoG filter. This filter was first introduced by Lindeberg [22] and is based on the image scale-space representation that allows for the detection of blob-like structures in images.

Given an input image $I(x, y)$, the Gaussian scale-space representation at a certain scale t is represented as:

$$
\begin{aligned}
L(x, y, t) &= g(x, y, t) * I(x, y) \\
g(x, y, t) &= \frac{1}{2\pi t} e^{-\frac{x^2 + y^2}{2t}},
\end{aligned} \tag{1}
$$

where $*$ is the convolution operator. Given this, the scale normalized LoG operator is defined as:

$$
\nabla^2 L(x, y, t) = t^2 (L_{xx}(x, y, t) + L_{yy}(x, y, t)), \tag{2}
$$

where L_{xx} and L_{yy} are the image second derivatives in x and y respectively, and t is the scale parameter so that $t = r/1.5$ for a particle radius r [11, 13].

It is known that the $\nabla^2 L$ has a strong positive response for dark blobs of size t and strong negative responses for bright blobs of similar size. However, and since possible variations on the immunogold particle structure can occur during the acquisition of the digital image of the biological sample (Figure 1), we have applied the LoG filter over a range of possible scale responses. Given the expected range of the immunogold particles radius, r, we filtered the images over the range $t = \{r_i/1.5 \mid \forall r_i \in \{r - \delta, \ldots, r + \delta\}\}$. Setting $\delta = 1$ provided the best results for our experiments [13]. We then perform the detection of immunogold particles by detecting local maxima in both spatial and scale dimensions over all LoG responses (Figure 2—center) in the input image (Figure 2—left). The detected maxima enabled us to estimate the position of immunogold particles (Figure 2—right). A sample of the LoG performance is depicted in Figure 2 for all datasets of this work: `db1` for the dataset of magnification `15000`, `db2` for the dataset of magnification of `20000`, `db3` for the dataset of magnification of `30000` and finally, `db4` for the dataset of magnification of `50000`. Among the LoG filter response and the respective detections, the erroneous detections provided by the LoG are also visible in Figure 2.

It can be claimed that other approaches can lead to similar (or even better results) than LoG. Such approaches encompass the Circular Hough Transform [24, 31] or variants of the Wavelets Transform [28]. One variant of the wavelets transform is publicly available in the bioimaging software identified as Spot Detector (SD) and which we have already mentioned above. The Circular Hough Transform is a particular case of the Hough Transform specially tailored for the detection of circular objects. In a nutshell, this method consists on fitting a circle for a given interest point. Applying these
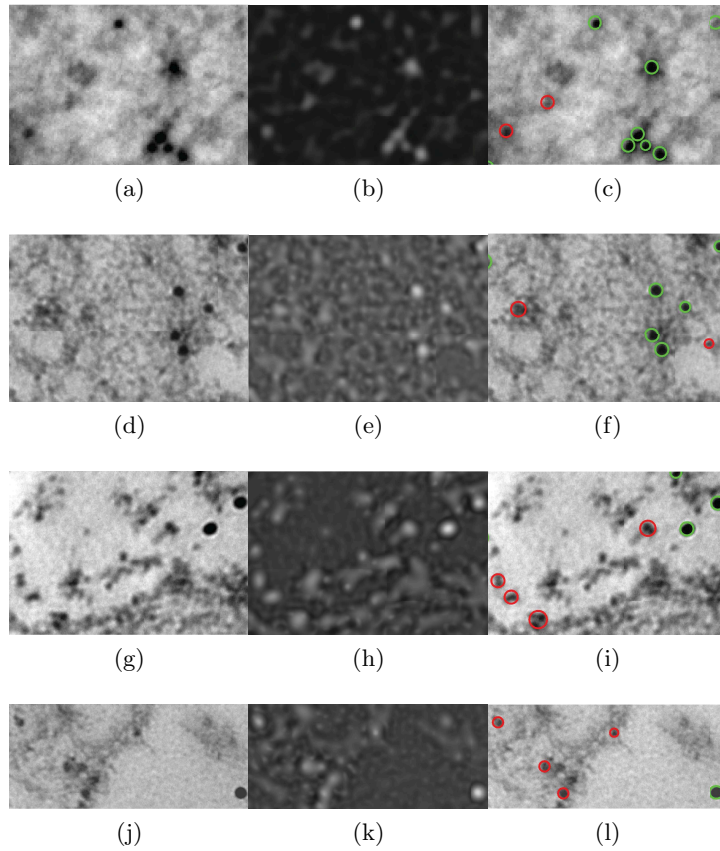
6

Figure 2: Immunogold particle detection based on the LoG filter. From top to bottom we have different detections from images with magnifications 15000 (db1), 20000 (db2), 30000 (db3) and 50000 (db4), respectively. For each row, on the left we have the original image followed in the center by the LoG response and finally on the right, the detections overlaid in the original image. In these samples we also show some false positive detections (in red) illustrating the difficulties of using the LoG filter alone (better viewed on color). Different sizes of the immunogold particles are related to the cropped region of the original image.

approaches to the immunogold particle detection problem rendered however a significant reduction of performance in comparison to the LoG. For these reasons, and since this sole approach can induce significant detection errors, we have focused on coupling a robust ML technique to the LoG filter.

7

3.2 Immunogold Recognition using Stacked Denoising Autoencoders

In order to speed-up the detection and recognition processes, the first step of our framework is performed by the LoG filter. We then processed the detections provided by the LoG, by employing a deep learning algorithm.

An AutoEncoder (AE) is, in the simplest form, a Neural Network (NN) with one hidden and one output layer that is designed to reconstruct its own input. As exemplified in Fig. 3(a), it is subject to two restrictions: the weight matrix of the output layer is the transposed of the weight matrix of the hidden layer and the number of output neurons is equal to the number of inputs [2].

The values of the hidden layer neurons, called the encoding, are obtained via Equation 3, where $\mathbf{x}$ is the input vector, s denotes the sigmoid function, $\mathbf{b}$ is the vector of hidden neuron biases, and $\mathbf{W}$ is the matrix of hidden weights. The values of the output neurons, called the decoding, are computed as in Equation 4, where $\mathbf{c}$ is the vector of output neuron biases. One advantage of the AEs is their ability to capture relevant information of the underlying distribution of the samples [33].

$$\mathbf{h}(\mathbf{x}) = s\left(\mathbf{b} + \mathbf{W}\mathbf{x}\right) \tag{3}$$

$$\hat{\mathbf{x}}(\mathbf{h}(\mathbf{x})) = s\left(\mathbf{c} + \mathbf{W}^T\mathbf{h}(\mathbf{x})\right) \tag{4}$$

Though AEs attain sparse features with good generalization capabilities, it is still required to have a model that captures good representations of the data. To achieve this goal the Denoising AutoEncoder (DAE) has been presented as a robust generalization of the AE. DAEs models are still designed to rebuild the original data but now from input data corrupted with noise. In practice, a small percentage of random components of $\mathbf{x}$ are set to zero [36]. Reconstruction of the input data is achieved by minimizing the reconstruction loss while allowing the DAEs to avoid a direct copy of the data [37]. These models had their robustness augmented by stacking (denoising) autoencoders (Fig. 3(b)). SDA gives the model the advantage of learning hierarchical features with low-level features represented at lower layers and higher-level features represented at upper layers [5, 37, Section 3]. One limitation of these "deep" models is concerned with the number of layers that one has to train and the total amount of time that it would take.

The breakthrough for training these models was achieved by conducting a layer-by-layer unsupervised training to find the proper initialization weights. This scheme allows the learning model to escape from local minima that is so common when training such networks [36]. This unsupervised training approach of the SDAs is usually referred to as pre-training (Fig. 3(b)). To perform a classification task, we add to the top of the network a logistic layer (Fig. 3(c)) and the entire network is then "fine-tuned" in order to minimize some classification loss function [2, 5].
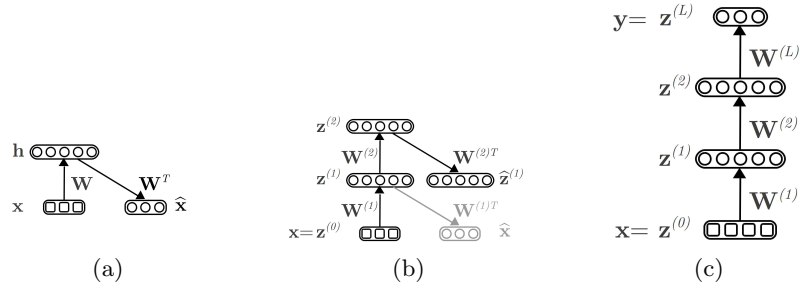
8

Figure 3: (a) An auto-encoder, (b) Pre-training of hidden layers of a deep network using auto-encoders. (c) A complete deep network with two hidden layers and an output layer. (Based on [21]).

SDAs are a very promising ML tool for the recognition of the circular shaped immunogold particles. A representative sample of the images that we used to train the SDA is depicted in Figure 4.
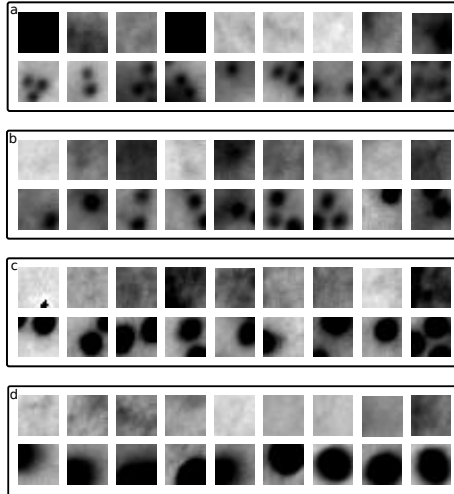

Figure 4: Different types of patches for all databases: (a) db1, (b) db2, (c) db3 and (d) db4. In each, the top row shows background, noise and artifacts and the bottom row shows immunogold particles.

Given the particular features of the immunogold particles, it is expected that an SDA captures relevant representations from these samples and easily discriminates the immunogold particles from the remaining artifacts or cellular structures. A far more complex scenario occurs when multiple immunogold particles are present in the same patch (i.e, a small window), (see Figure 4), especially in low magnifications such as in the 15000 magnification. In this case an SDA has to be able to deal with a variable number of particles in the same patch. Thereby, an SDA is trained to recognize par-

ticles belonging to a given magnification. To strengthen the robustness of this model to noise and other artifacts we train it by corrupting the training samples with noise. Once the best model is obtained it will consider the estimates provided by the LoG. The SDA thus considers a patch of the image centered in the location given by LoG to output the final prediction.

4 Transfer Learning for the Recognition of Immunogold Particles

TL aims to transfer a learning model that was acquired in one problem, the source problem, onto another problem, the target problem, dispensing with the bottom-up construction of the target model [34]. With this, TL algorithms aim to overcome one of the major drawbacks of ML: limited labelled data. There is another advantage of using TL algorithms: reduction of development and computational times for learning (training) models for new (target) problems. TL algorithms embedded in DNNs have already shown interesting features such as better generalization capabilities and reduced training times as shown in other works [18] (and references therein).[1]

As it was clear in the previous Section, our models' performance is also bounded by the quality of the dataset (and its annotations). For instance, on datasets with low-magnifications (i.e., 15000) we have noise and complex structures. Ergo, we obtain a feeble performance or high variances for the recognition of particles on such low-magnifications mostly because of those artifacts. For this scenario the advantage on using TL should be obvious: to transfer a model that was obtained on a higher magnification to a dataset of a lower magnification. Consequently, TL presents itself as an appealing alternative. Under this broad topic there has been a diverse set of methods being proposed: Never-ending learning [35], covariate shift (ref. [20] in [29]), weighting instance (ref. [6] in [29]) and unsupervised TL (ref. [26] in [29, 26]) are just a small set of methodologies presented in the literature. See [29] for a broader analysis. DNNs have raised some interesting questions within this research topic. Concretely, how can we devise DNNs for TL and what are the best strategies for these algorithms [17, 34]. On the other hand, Patricia *et al.* proposed in [30] a single Support Vector Machine formulation to solve the different types of TL settings. Beker *et al.* in [4] worked on the application of TL to Microscopy Imaging and presented a covariate shift approach for the recognition of Cellular Structures using a set of week classifiers. However, the experimentations and adaptability of TL has been limited to the analysis of Mitochondria.

In this Section we will describe our framework under TL consisting on the following points: (a) An SDA is first trained to distinguish immunogold particles from cluttered background; (b) This model is then reused on

---

[1]Check also the website: `http://www.deepnets.ineb.up.pt`

another problem (with a different magnification); and, (c) Models are then assessed for the detection task.

Low-magnifications (e.g., magnification of 15000) are usually used by a life-scientist for identifying regions of interest in EM. Even though these acquisitions are afterwards discarded to perform a more in-depth analysis, they contain rich information that can expedite many of the quantifications that have to be conducted for a given experiment. By directly exploring images obtained at lower magnifications we can attain reduced experimentation costs, image acquisition and labelling times. However, an automatic learning model is prone to misclassify a large set of patches due to the noise and artifacts present in the dataset (we will see some of these effects shortly). To overcome this undesirable outcome, we can build a learning model using a dataset with a high magnification as source problem (e.g., 50000, containing well defined immunogold particles and without clusters of immunogold particles), and transfer it to a target problem of a dataset with a low magnification (e.g., 15000). Putting it simply, layer weights for the target model are initialized with the values of the source model. Learning (of the target problem) can be conducted in several ways: (a) by fixing the layer weights of the network or by letting them readjust through the minimization of the reconstruction error (pre-training); (b) by fixing or letting the network relearn and thus letting it to readjust the decision function (fine-tune); or (c) a mixture of both [18, 16, 1, 5, 3] (and references therein) — see Algorithm 1 for a brief presentation.

For the purpose of this work, we considered the (b) approach above described. In our experimental work we have analyzed the impact of the reusability of the different hidden layers. In fact, and for the immunogold particle recognition, one may argue that the major changes will occur at a feature level thanks to the changes of the magnification of the immunogold particles. Looking carefully at Figure 1 we can see that this seems to be the case. Therefore, the recognition performance of the immunogold particles through TL would have significant impact by relearning only the first layers of the network. The analysis of the effects of relearning specific parts of the network architecture will be addressed in more detail in Section 5.

5   Experimental Study for Immunogold Detection and Recognition

In this Section we will thoroughly describe the experimental work that we have conducted as well as a detailed discussion on the results that were obtained. The code is publicly available[2]. Our study is split into two halves: first, the detection by coupling the SDA with the LoG filter and second, the recognition of immunogold particles.

---

[2]Available at `http://www.deepnets.ineb.up.pt`

Algorithm 1: Pseudocode for training a TL model using an SDA for the recognition of immunogold particles.

1: **Input**: $\mathcal{M}_S$, an SDA model trained on a source problem and h_{TL}, the hidden layers that one wishes to reuse.
2: **Output**: $\mathcal{M}_T$, an SDA model obtained through TL for the target problem.
3: $\mathcal{M}_T \leftarrow \mathcal{M}_S$ `/* Copy the source model` `*/`
4: Let $\mathcal{H}$ be the set of hidden layers of $\mathcal{M}_S$ (or $\mathcal{M}_T$) and $h = h_{TL} \setminus \mathcal{H}$;
5: Discard the hidden-layers h of the SDA target model, $\mathcal{M}_T$;
6: $\mathcal{M}_T \leftarrow$ `FineTuneNetwork` $(\mathcal{M}_T, h)$;

Immunogold Particles Dataset: This novel dataset results from a study of the composition of cell wall ingrowths of maize endosperm transfer cells via the detection and quantification of immunogold particles. As previously stated, images with lower magnification allow a wider field of view but the detection of the immunogold particles is much more difficult than with higher magnifications. The purpose was to develop an automated system that could be able to detect particles in lower magnification images with a comparable performance to that obtained with higher magnification images. The dataset contains 100 images with 4008 pixels wide and 2670 pixels tall. All images were acquired using a Transmission Electron Microscopy (TEM) JEOL JEM 1400 with a GATAN Orius SC10000A2 CCD. These images were recorded in four different magnifications: 15000 (scale of $1\mu m$ to the size of the image), 20000 ($0.5\mu m$), 30000 ($0.5\mu m$) and 50000 ($200nm$) from different biological samples (see Figure 1) whereas a manual annotation was conducted with the plugin 'manual counting' provided by Icy software [7]. Each magnification corresponds to a single dataset (see Table 1). The datasets are publicly available on our website.

Performance Measures: The detection performance of the LoG filter was conducted by assigning a ground-truth to a given detection if the Euclidean distance between the ground-truth and the detected point positions is below the size of the particle radius r. Of course, we ensure that there is a one-to-one mapping between detection and ground-truth. To measure the performance of the automatic detections we used the following metrics:

- True Positive (TP): number of correctly detected immunogold particles;

- False Positive (FP): number of falsely detected immunogold particles;

- False Negative (FN): number of immunogold particles which were not detected.

The performance of our method was plotted in a Precision-Recall curve [10] as follows:

$$\text{Precision} = \frac{TP}{TP + FP}, \qquad \text{Recall} = \frac{TP}{TP + FN} \qquad (5)$$

We will also summarize the performance results of our methods by using the F-measure which combines both precision and recall. This measure is given as follows:

$$\text{F-measure} = 2 \cdot \frac{\text{Precision} \cdot \text{Recall}}{\text{Precision} + \text{Recall}} \qquad (6)$$

5.1 Detection and Recognition of Immunogold Particles

Our experimental study starts by first constructing an SDA model. We extract patches with 20×20 pixels from 60% of our dataset (60 images, 15 samples per magnification) half of them containing all the immunogold particles and the other half containing background, cellular structures or other artifacts — see Table 1. A patch could contain more than one particle and/or portions of several other particles (see Figure 4). Finally, patches are labelled as containing at least one immunogold particle if the Euclidean distance between the patch position (on the image) and the position of the annotation is below the size of the patch. Pixel values of the patches were normalized to be within $[0, 1]$. To find the best parametrization of the SDA model we have performed a grid search on the pre-training learning rate $[0.01, 0.001]$ and fine-tune learning rate $[0.1, 0.01]$. We fixed the number of neurons to 1000 units per layer and the number of hidden layers was also fixed to 3. The grid search was conducted by carrying out a three-fold cross-validation in the training set and performance assessed in the validation set. The corruption level was set to 10% across all hidden layers. Pre-train and fine-tune epochs were set to 1000 and 3000, respectively, and all models were trained by batches. For the `db1` we used 1000 patches per batch and for the `db2`, `db3` and `db4` we used 100 patches per batch. For the execution of our TL experiments, we had to resize by half the images of the datasets `db3` and `db4` to afterwards use them as source problem (more details for this results will be described thoroughly in Section 5.2). Note, however, that patches used to train our models had the same dimension, i.e., 20×20 pixels. Our models were developed and tested using the Theano framework [3, 6] with simulations being executed on a GTX 980 GPU on a i7-5930K CPU with 16Gb of RAM. Test results of the SDA are depicted in Table 2.

Once we obtained the best SDA model, we proceeded with the development of the LoG filter. LoG is solely controlled by the scale parameter which we have set to vary between known values of the immunogold particles size: $[3, \ldots, 13]$ pixels. For experimental swiftness, and since some particle radius could not make sense for a given magnification, we trimmed the search space for an "optimum" radius value. Thus, the radius range was set to $\{3, 4, 5\}$,

Table 1: Size and magnification of each dataset used to train our models. Datasets are balanced being composed by the same number of immunogold particles (objects) and cellular structures or other artifacts (background).

	db1	db2	db3	db4
Number of instances	16556	10766	5060	1644
Magnification	15000	20000	30000	50000

Table 2: Baseline results for the recognition of immunogold particles with SDAs. We also include the pre-training and fine-tuning times for training this model (average time per repetition).

Dataset	Accuracy	Pre-training Time (sec.)	Fine-Tuning Time (sec.)
db1	79.1 ± 5.6	225.1 ± 44.5	30.0 ± 49.3
db2	96.0 ± 1.4	245.3 ± 51.0	367.8 ± 81.6
db3	87.1 ± 12.6	135.7 ± 18.6	183.5 ± 78.1
db4	91.5 ± 5.2	33.7 ± 10.0	54.3 ± 8.0

$\{3, 5, 7, 9\}$, $\{5, 7, 9, 11\}$ and $\{9, 11, 13\}$, pixels, for images of the datasets db1 to db4, respectively.

We also measured the performance for each threshold applied to the filter response. This was done by ranging the values of the threshold between 5 and 55. The threshold set had to be adjusted for a given magnification: $\{10, 15, 20, 25\}$ for db1 and db2 and, $\{5, \ldots, 45\}$ with steps of 5 for db3 and $\{5, \ldots, 55\}$ also with steps of 5 for the db4. To find the best parameterization we have performed a three-fold cross validation with the *same* 60% of the total number of images (60 images, 15 samples per magnification) as in with the SDA for training our LoG model and with the *same* 40% for evaluating its performance. In other words, the learning process was conducted independently from the LoG training, but using the same images. The performance of the LoG is represented by a Precision-Recall curve on the validation set [10] and results are shown in Figure 5.

This framework works as follows: Given a test image we first apply the LoG filter to obtain the initial estimates of the immunogold particles position. Afterwards, we extract a patch with 20×20 pixels centered at the position of the LoG detection. This patch is afterwards evaluated by the SDA that we developed before. Finally, we assessed the variability of our methods' performance by repeating the experiment 20 times by shuffling the dataset.

For the magnification of 15000 — see Figure 5a, we observed that the expected immunogold particle radius tested during the detection of immuno-

gold particles attained the best results ($radius = 3$ and 4). Comparing to the other radius tested, with $radius = 3$ (or 4) it achieved a higher recall, which means a higher number of immunogold particles were detected. A similar analysis can be performed for the remaining figures stating the importance of the size of the radius. Moreover, by having one single parameter this method is intuitive and easy to use though prone to some error as it is expressed by the low precision rates. Another important result is that when using higher magnifications, 30000 and 50000, we can obtain very good results only with the LoG filter. This behavior is related to the quality of the images which contain little noise and artifacts. Moreover, these datasets also contain immunogold particles far apart from each other, making them easy to detect. Unfortunately, when working with such high magnifications (e.g., 50000) the field-of-view is reduced significantly. Thus, working with such high magnifications may be useful only after determining the regions of interest.

5.2 Evaluation of TL for the Recognition of Immunogold Particles

As it was mentioned, one advantage of using TL algorithms is that it eliminates the need to redesign learning models for a distinct, but related, problem. In our case, since we are using several magnifications of EM images, we explore different TL settings for the recognition of immunogold particles of Maize cells.

The experimental procedure to train the baseline models was conducted as described above in Section 5.1. We then proceeded with the TL approach. Images of the dataset db4 were resized to half (keeping the aspect ratio), but maintaining the size of the patches (20×20). This led to immunogold particles with a radius around 7 pixels (recall that the radius size of immunogold particles on the dataset db1, was 4 pixels). If we do not resize the images of the source problem we do obtain some accuracy improvements but lower than the ones when resizing the source problem. TL can be conducted by reusing the first layer of the source model and by fine-tuning only the remaining layers to the target model (coded [011]); another possibility is reusing the first and second layers and fine-tuning the last layer ([001]). By reusing the full source network ([000]) the model would not suffer changes, and thus would have not been fine-tuned to the target problem. Results for all variations of the TL settings are presented in Table 3.

Results in Table 3 show that all of the TL settings improve the baseline result (79%). The accuracy improvement is at least 10%. As mentioned before, the low accuracy rate of the target problem is related to the high variability of the particles and image artifacts. This causes a severe underperformance on the network. By learning the source problem dataset db4, we are thus providing a better starting point for the model to learn the

Table 3: Results of the application of TL to the recognition of immunogold particles. The baseline model was trained in a standard ML way on the dataset with magnification of `15000` (target problem). A model trained for the dataset with magnification of `50000` (source problem, immunogold particles were resized) was obtained and reused on the target problem. Overall, all TL approaches achieved an improvement of more than 10%. Each layerwise TL strategy is illustrated in the column TL setting (see main text). Results were averaged over 20 repetitions.

Method	Source (re-sized)	Target	Reusability and Fine-Tuning (TL) Setting	Accuracy ($\pm$ std. dev)	Pre-Training + Fine-Tuning Time (sec.)
Baseline	-	db1	-	79.1 ± 5.6	255.1 ± 83.0
TL	db4	db1	[011]	90.9 ± 3.5	144.9 ± 82.9
TL	db4	db1	[001]	89.9 ± 3.6	152.0 ± 55.7
TL	db4	db1	[110]	91.8 ± 3.7	138.7 ± 89.1
TL	db4	db1	[100]	91.0 ± 4.2	131.0 ± 84.0
TL	db4	db1	[111]	91.8 ± 3.1	158.1 ± 90.8

target problem. In fact, transferring the model and letting all layer weights be fine-tuned ([111]) to the target problem achieved the best result (approx. 92%). Another result from our experimental study is concerned with the relevance of the feature representation that the network has captured. From Table 3 we can infer that the first layers are the most relevant. In fact, letting the first two layers of the network be re-learnt and fixing only the last layer (TL setting [110]) achieved a higher performance (approx. 92%) in comparison with only re-learning the last layer ([001] with an accuracy of 90%).

A similar experience was conducted when using `db3` as source problem. Once again, reusing and fine-tuning the full network (reusability setting [111]) lead to the best results in comparison to the baseline: 13% improvement of performance accuracy. Such results are depicted in Table 4. A similar conclusion can be obtained when using the dataset `db2` as source problem (see Table 5). Reusing and fine-tuning all layers of the network rendered the best results with 93.3% of accuracy performance. Overall, using any TL setting for learning the immunogold problem outperformed the baseline (79% for the dataset `db1`).

We have also tested the applicability of the TL models over the detections provided by LoG. In a first experiment `db4` was defined as source problem and `db1` as target problem. Once the learning model for the source problem was obtained, we have applied it to the detections provided by the LoG filter. Results are depicted in Table 6.

Table 4: Results of the application of TL to the recognition of immunogold particles. The baseline model was trained in a standard ML way on the dataset with magnification of 15000 (target problem). A model trained for the dataset with magnification of 30000 (source problem, immunogold particles were resized) was obtained and reused on the target problem. Overall, all TL approaches achieved an improvement of more than 10%. Each layer-wise TL strategy is illustrated in the column TL setting (see main text). Results were averaged over the 20 repetitions.

Method	Source (re-sized)	Target	Reusability and Fine-Tuning (TL) Setting	Accuracy (± std. dev)	Pre-Training + Fine-Tuning Time (sec.)
Baseline	-	db1	-	79.1 ± 5.6	255.1 ± 83.0
TL	db3	db1	[011]	91.4 ± 5.9	166.1 ± 84.8
TL	db3	db1	[001]	89.8 ± 8.2	119.5 ± 77.4
TL	db3	db1	[110]	91.1 ± 6.3	152.2 ± 95.3
TL	db3	db1	[100]	87.7 ± 12.8	121.2 ± 97.0
TL	db3	db1	[111]	92.3 ± 4.6	220.1 ± 56.0

Table 5: Results of the application of TL to the recognition of immunogold particles. The baseline model was trained in a standard ML way on the dataset with magnification of 15000 (target problem). A model trained for the dataset with magnification of 20000 was obtained and reused on the target problem. Overall, all TL approaches achieved an improvement of more than 10%. Each layer-wise TL strategy is illustrated in the column TL setting (see main text). Results were averaged over the 20 repetitions.

Method	Source	Target	Reusability and Fine-Tuning (TL) Setting	Accuracy (± std. dev)	Pre-Training + Fine-Tuning Time (sec.)
Baseline	-	db1	-	79.1 ± 5.6	255.1 ± 83.0
TL	db2	db1	[011]	92.9 ± 2.9	304.3 ± 129.0
TL	db2	db1	[001]	92.4 ± 2.9	194.9 ± 123.6
TL	db2	db1	[110]	92.9 ± 3.3	290.6 ± 116.5
TL	db2	db1	[100]	92.1 ± 4.0	251.3 ± 146.5
TL	db2	db1	[111]	93.3 ± 2.9	326.1 ± 78.1

Table 6: F-measure performance for the best Precision and Recall for LoG and LoG coupled with SDA (see Figure 5). Best results are in bold and presented in percentage. Results were averaged over the 20 repetitions.

	LoG	LoG+SDA	LoG+SDA by TL [111]		
	-	-	Source Problem: db4	Source Problem: db3	Source Problem: db2
db1	84.2 (1.5)	83.9 (2.3)	**85.4 (1.7)**	**85.2 (1.9)**	**85.4 (1.7)**

As mentioned, the reduced training times is one of the many advantages for using TL strategies. In particular for DNNs the gains can be significantly high due to the time that it takes in such deep (big) networks. Training an SDA for the baseline (target) problem (i.e., dataset db1) took on average 255 seconds. When using TL with the dataset db4 as source problem, the training time is reduced to 158 seconds (reusing and fine-tuning all layers of the network — see Table 3). In other words, we obtain a reduction of 38% on the training time. This indeed shows the advantage on using TL as a way to speed-up the training time. When using the dataset db3 as source problem and, reusing and fine-tuning all layers of the network (see Table 4) for the dataset db1 takes in average 220 seconds. In short, if one wishes to solve the db1 one ought use the db4 as source problem. Solving db1 by TL will take 239.8 seconds corresponding to the total time of training the baseline model of db4 plus the TL training time. It still takes less time than training the db1 baseline model and with an increased accuracy performance improvement.

6   Conclusions

In this work we proposed a framework for the automatic detection of immunogold particles in different magnifications. We found that solely the LoG filter attained results of over 84% of accuracy with the F-measure. Regarding TL for immunogold recognition, the conclusions of our study are two-fold: a) there was a significant accuracy improvement when applying TL (around 10% of improvement); and, b) a reduction in training times. Overall, to solve the problem of immunogold recognition on low magnifications (i.e., magnification of 15000, db1) it is better to use as source problem the dataset db4, magnification 50000.

These results show that these approaches are also resilient to the presence of noise, artifacts and cluttered background and are easy to set-up based on the few parameters of the framework (only dependent on the threshold parameter of the LoG filter response). These methods can help a bio-researcher in the tedious and time-consuming task of identifying immunogold particles

in large EM images.

We also make available the developed code and the dataset used such that our work can be reproduced and improved by the community.

7   Acknowledgements

References

[1] Amaral, T., Silva, L.M., Alexandre, L.A., Kandaswamy, C., de Sá, J.M., Santos, J.: Improving Performance on Problems with Few Labelled Data by Reusing Stacked Auto-Encoders. In: ICMLA (2014)

[2] Amaral, T., Silva, L.M., Alexandre, L.A., Kandaswamy, C., Santos, J.M., de Sá, J.M.: Using different cost functions to train stacked auto-encoders. In: Artificial Intelligence (MICAI), 2013 12th Mexican International Conference on. pp. 114–120. IEEE (2013)

[3] Bastien, F., Lamblin, P., Pascanu, R., Bergstra, J., Goodfellow, I.J., Bergeron, A., Bouchard, N., Bengio, Y.: Theano: new features and speed improvements. Deep Learning and Unsupervised Feature Learning NIPS 2012 Workshop (2012)

[4] Becker, C., Christoudias, C., Fua, P.: Domain adaptation for microscopy imaging. Medical Imaging, IEEE Transactions on PP(99), 1–1 (2014)

[5] Bengio, Y.: Deep learning of representations for unsupervised and transfer learning. Journal of Machine Learning Research-Proceedings Track 27, 17–36 (2012)

[6] Bergstra, J., Breuleux, O., Bastien, F., Lamblin, P., Pascanu, R., Desjardins, G., Turian, J., Warde-Farley, D., Bengio, Y.: Theano: a cpu and gpu math expression compiler. In: Proceedings of the Python for scientific computing conference (SciPy). vol. 4, p. 3. Austin, TX (2010)

[7] de Chaumont, F., Dallongeville, S., Chenouard, N., Hervé, N., Pop, S., Provoost, T., Meas-Yedid, V., Pankajakshan, P., Lecomte, T., Le Montagner, Y., et al.: Icy: an open bioimage informatics platform for extended reproducible research. Nature methods 9(7), 690–696 (2012)

[8] Ciresan, D., Giusti, A., Gambardella, L., Schmidhuber, J.: Neural networks for segmenting neuronal structures in em stacks. vol. 1, p. 3 (2012)

[9] Ciresan, D., Giusti, A., Gambardella, L.M., Schmidhuber, J.: Deep neural networks segment neuronal membranes in electron microscopy images. In: Advances in neural information processing systems. pp. 2843–2851 (2012)

[10] Davis, J., Goadrich, M.: The relationship between precision-recall and roc curves. In: Proceedings of the 23rd international conference on Machine learning. pp. 233–240. ACM (2006)

[11] Esteves, T., Oliveira, M.J., Quelhas, P.: Cancer cell detection and morphology analysis based on local interest point detectors. In: Sanches, J.M., Micó, L., Cardoso, J.S. (eds.) Pattern Recognition and Image Analysis, Lecture Notes in Computer Science, vol. 7887, pp. 624–631. Springer Berlin Heidelberg (2013)

[12] Fisker, R., Carstensen, J.M., Hansen, M.F., Bødker, F., Mørup, S.: Estimation of nanoparticle size distributions by image analysis. Journal of Nanoparticle Research 2(3), 267–277 (2000)

[13] Gamelas Sousa, R., Esteves, T., Rocha, S., Figueiredo, F., Quelhas, P., Silva, L.M.: Automatic Detection of Immunogold Particles from Electron Microscopy Images. LNCS 9164, pp. 377–384 (2015).

[14] Huang, T., Hacker, C., Lucocq, J., McKenna, S.J.: Detecting and segmenting nanodiscs in immuno-electron micrographs. In: Medical Image Understanding and Analysis (MIUA). pp. 53–58 (2014)

[15] Jorstad, A., Fua, P.: Refining mitochondria segmentation in electron microscopy imagery with active surfaces. In: European Conference on Computer Vision (ECCV) Workshop on Non-Rigid Shape Analysis and Deformable Image Alignment. No. EPFL-CONF-201868 (2014)

[16] Kandaswamy, C., Silva, L.M., Alexandre, L.A., Santos, J.M., de Sá, J.M.: Improving deep neural network performance by reusing features trained with transductive transference. In: Artificial Neural Networks and Machine Learning–ICANN 2014. pp. 265–272. Springer (2014)

[17] Kandaswamy, C., Silva, L.M., Alexandre, L.A., Sousa, R., Santos, J.M., de Sá, J.M.: Improving transfer learning accuracy by reusing stacked denoising autoencoders. In: Systems, Man and Cybernetics (SMC), 2014 IEEE International Conference on. pp. 1380–1387. IEEE (2014)

[18] Kandaswamy, C., Silva, L.M., Alexandre, L.A., Sousa, R., Santos, J., de Sá, J.M.: Improving transfer learning accuracy by reusing stacked denoising autoencoders. In: Proceedings of the IEEE SMC Conference (2014)

[19] Kang, B.H., Xiong, Y., Williams, D.S., Pozueta-Romero, D., Chourey, P.S.: Miniature1-encoded cell wall invertase is essential for assembly and function of wall-in-growth in the maize endosperm transfer cell. Plant physiology 151(3), 1366–1376 (2009)

[20] Knott, G., Genoud, C.: Is EM dead? Journal of cell science 126(20), 4545–4552 (2013)

[21] Larochelle, H., Erhan, D., Courville, A., Bergstra, J. and Bengio, Y.: An empirical evaluation of deep architectures on problems with many factors of variation. In International Conference on Machine Learning (ICML), pages 473–480 (2007)

[22] Lindeberg, T.: Scale-space theory: A basic tool for analyzing structures at different scales. Journal of Applied Statistics 21(2), 224–270 (1994)

[23] Lucchi, A., Smith, K., Achanta, R., Knott, G., Fua, P.: Supervoxel-based segmentation of mitochondria in em image stacks with learned shape features. Medical Imaging, IEEE Transactions on 31(2), 474–486 (2012)

[24] Luo, D., Smart, P., Macleod, J.E.: Circular hough transform for roundness measurement of objects. Pattern recognition 28(11), 1745–1749 (1995)

[25] Mallick, S.P., Zhu, Y., Kriegman, D.: Detecting particles in cryo-em micrographs using learned features. Journal of Structural Biology 145(1), 52–62 (2004)

[26] Mesnil, G., Dauphin, Y., Glorot, X., Rifai, S., Bengio, Y., Goodfellow, I.J., Lavoie, E., Muller, X., Desjardins, G., Warde-Farley, D., et al.: Unsupervised and transfer learning challenge: a deep learning approach. ICML Unsupervised and Transfer Learning 27, 97–110 (2012)

[27] Monjardino, P., Rocha, S., Tavares, A.C., Fernandes, R., Sampaio, P., Salema, R., da Câmara Machado, A.: Development of flange and reticulate wall ingrowths in maize (*Zea mays* L.) endosperm transfer cells. Protoplasma 250(2), 495–503 (2013)

[28] Olivo-Marin, J.C.: Extraction of spots in biological images using multiscale products. Pattern Recognition 35(9), 1989–1996 (2002)

[29] Pan, S.J., Yang, Q.: A survey on transfer learning. Knowledge and Data Engineering, IEEE Transactions on 22(10), 1345–1359 (2010)

[30] Patricia, N., Caputo, B.: Learning to learn, from transfer learning to domain adaptation: a unifying perspective. In: Computer Vision and Pattern Recognition (CVPR), 2014 IEEE Conference on. pp. 1442–1449. IEEE (2014)

[31] Pei, S.C., Horng, J.H.: Circular arc detection based on hough transform. Pattern recognition letters 16(6), 615–625 (1995)

[32] Ribeiro, E., Shah, M.: Computer vision for nanoscale imaging. Machine Vision and Applications 17(3), 147–162 (2006)

[33] Rifai, S., Vincent, P., Muller, X., Glorot, X., Bengio, Y.: Contractive auto-encoders: Explicit invariance during feature extraction. In: Proceedings of the 28th International Conference on Machine Learning (ICML-11). pp. 833–840 (2011)

[34] Sousa, R.G., Esteves, T., Rocha, S., Figueiredo, F., de Sá, J.M., Alexandre, L.A., Santos, J.M., Silva, L.M.: Transfer Learning for the Recognition of Immunogold Particles in TEM Imaging. In: Rojas, I., Joya, G., Catala, A. (eds.) Advances in Computational Intelligence. Lecture Notes in Computer Science, vol. 9094, pp. 374–384. Springer International Publishing (2015)

[35] Thrun, S.: Learning to learn: Introduction. In: In Learning To Learn. Citeseer (1996)

[36] Vincent, P., Larochelle, H., Bengio, Y., Manzagol, P.A.: Extracting and composing robust features with denoising autoencoders. In: Proceedings of the 25th International Conference on Machine Learning. pp. 1096–1103. ICML '08, ACM, New York, NY, USA (2008)

[37] Vincent, P., Larochelle, H., Lajoie, I., Bengio, Y., Manzagol, P.A.: Stacked denoising autoencoders: Learning useful representations in a deep network with a local denoising criterion. The Journal of Machine Learning Research 11, 3371–3408 (2010)

[38] Voss, N., Yoshioka, C., Radermacher, M., Potter, C., Carragher, B.: Dog picker and tiltpicker: software tools to facilitate particle selection in single particle electron microscopy. Journal of Structural Biology 166(2), 205–213 (2009)

[39] Wang, R., Pokhariya, H., McKenna, S.J., Lucocq, J.: Recognition of immunogold markers in electron micrographs. Journal of Structural Biology 176(2), 151 – 158 (2011)

[40] Woolford, D., Hankamer, B., Ericksson, G.: The laplacian of gaussian and arbitrary z-crossings approach applied to automated single particle reconstruction. Journal of structural biology 159(1), 122–134 (2007)
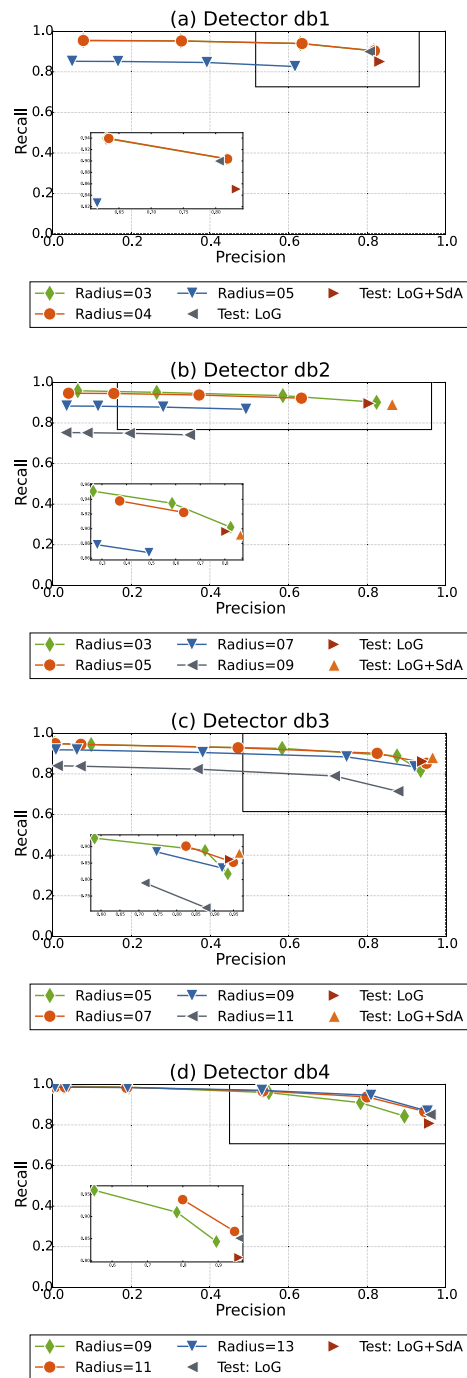
Figure 5: Precision-Recall curves averaged over 20 repetitions for the LoG on the validation set. Non-connected points correspond to the test results for LoG and LoG+SDA. Upper right areas of interest in each graph is zoomed in larger rectangles for visualization purposes.

This figure "auto-encoders-a.png" is available in "png" format from:

http://arxiv.org/ps/1712.02824v1

This figure "auto-encoders-b.png" is available in "png" format from:

http://arxiv.org/ps/1712.02824v1

This figure "auto-encoders-c.png" is available in "png" format from:

http://arxiv.org/ps/1712.02824v1